RSC Advances

Hollow Co₃O₄ microspheres with nano-sized shell: One-step large-scale synthesis, Growth mechanism and Supercapacitor properties

Chao Feng[1], Jinfeng Zhang[1], Yida Deng[2]*,Cheng Zhong[2], Lei Liu[1], Wenbin Hu[1,2]*

1. State Key Laboratory of Metal Matrix Composites, School of Material Science and Engineering, Shanghai Jiao Tong University, Shanghai 200240, People's Republic of China

2. School of Material Science and Engineering, TianjinUniversity, Tianjin300072, People's Republic of China

Abstract

Hollow Co_3O_4 microspheres with thin spherical shell were produced with one-step method at a low hydrothermal temperature (120 ℃)，which could be obtained without the use of solid template, organic reagent and subsequent calcination. These hollow Co_3O_4 microspheres possess a diameter of ca. 500 nm and thin shell thickness of ca. 50 nm. The samples were characterized by field emission scanning electron microscope (SEM), transmission electron microscopic (TEM) and powder X-ray diffraction (PXRD). A multistep-splitting growth mechanism was proposed here to reveal the formation of hollow Co_3O_4 microspheres. The successful fabrication of hollow spherical morphology of these microspheres highlighted the H_2O_2 dosage and the nitrate concentration. The electrochemical performance tests of as-prepared samples indicated that the hollow Co_3O_4 microspheres exhibited ultrahigh specific capacitance of 1227, 1169, 1116, 1035 F/g at current densities of 1, 2, 4, 8 A/g, respectively. After 1000 cycles, the specific capacitance of hollow Co_3O_4 microspheres showed high charge/discharge reversibility and only slightly decayed

less than 3% at a current density of 2 A/g.

1. Introduction

To meet the ever-expanding energy demand in the new industrial age, research has been intensely undertaken to explore high capacity and power substitute electrode materials of traditional carbon striving to improve the efficiency of energy utilization.[1-9] Nowadays the hotspot has been focused on two main aspects: a) chemical modification and embellishment for traditional carbon becomes a common practice, for example, adopt carbon nanotubes (CNTs) , graphene or other materials with high electrochemical activity seems to be one of the appropriate options; b) other pseudocapacitance materials which store energy on the basis of fast reversible redox reactions occurring within those eletroactive materials owing to several oxidation states.

As a result, various transitional-metal oxides as a class of ideal materials have drawn intense attentions mainly due to their good specific capacitance,[10] long cycle life and a fast redox kinetics.[11] For instance, RuO_2,[12, 13] Co_3O_4,[14] NiO,[15, 16] MnO_2[17, 18] are considered to be the most desirable candidate materials for electrochemical capacitors (ECs) application. Recent studies revealed that Co_3O_4 is a promising alternative choice for carbon-base materials on account of the high capacitance (theoretical value to 3560 F/g), excellent reversible redox behavior, good corrosion stability and benign environmental friendliness.[19] On any condition, in order to improve the electrochemical performance of materials, seeking the design of higher specific surface area and easier electrolyte-accessibility seems to be the most possible

approach. Because the unique structures facilitate the ion diffusion and mitigate the

expansion of the lattice spacing of electrode materials, countless attempts have been

taken to synthesize Co_3O_4 of different morphologies such as wires,[20, 21] tubes,[22]

walls,[23] urchin-like structures.[24] Nevertheless, in consideration of the thermal stress

influence during the continuous electrochemical test, hollow morphology may

probably be the most stable structure from the point of view of structural and thermal

stability. Based on this viewpoint, researchers have devoted themselves to develop

hollow Co_3O_4 nanoparticles with varieties of techniques.[25, 26] However, there were

still obstacles block on the road of manufacturing hollow Co_3O_4 spheres in a

comparatively simple and efficient way. On one hand, in Ma's and Xiao's teamwork,

they both prepared hollow Co_3O_4 spheres or 3D hierarchical Co_3O_4twin-spheresby

annealing unchin-like hollow $Co(CO_3)_{0.5}(OH)•0.11H_2O$ which acted as the precursor

of morphology template[27]. The spherical morphology has been damaged to some

extent caused by the calcining process. On the other hand, in Sun's latest work, they

had to decorate the hollow Co_3O_4 nanospheres with graphene in the aim of improving

the electrochemical performance of Co_3O_4, thus increased the application costs and

complicated the preparation procedures.[28] Therefore, it still remains a huge chanllenge

to synthesize high performance hollow Co_3O_4 spheres with a low cost and effective

way.

In this article, we prepared hollow Co_3O_4 microspheres without the assist of solid

template and a subsequent calcination process. As is known that for the synthesis of

Co_3O_4 through various means, the oxidation of Co (II) to Co (III) remains as an

unable evaded obstacle. For purpose of solving this problem, previous researchers either adopt electrodeposition method or hydrothermal process followed by high temperature calcination. In this study, the main innovation of the synthesis hollow Co_3O_4 microspheres not only lay in taking advantages of the easy oxidation of $Co(NH_3)_6{}^{2+}$ to realize $Co^{2+} \rightarrow Co^{3+}$ in low temperature (120 ℃)，but also paid attention to manufacturing hollow structures with help of air bubbles. Moreover, the electrochemical performances of hollow Co_3O_4 microspheres exhibited ultrahigh specific capacitance of 1227, 1169, 1116 and 1035 F/g at current densities of 1, 2, 4, 8 A/g, respectively. The supercapacitor constructed with hollow Co_3O_4 microspheres also showed an excellent reversibility with an efficiency of 97.5% after 1000 cycles at a current density of 2 A/g. The amazing electrochemical properties could be ascribed to the greatly increased active sites and greatly shortened ion diffusion distances of this hollow structure.

2. Experimental Section

2.1 Materials

Cobalt nitrate ($Co(NO_3)_2$, analytical grade), sodium nitrate ($NaNO_3$, ≥ 99.5%), ammonium hydroxide ($NH_3 \cdot H_2O$, 25%~28%)，hydrogen peroxide (H_2O_2, 30%) were used. All reagents were pruchased from Sinopharm Chemical Reagent Co., Ltd. and were used as received. The deionized water used in all experiments with a resistivity of 18.2 MΩ•cm was prepared using an ultrapure water system (Millipore).

2.2 Preparation of hollow Co_3O_4 microspheres

In a typical synthesis, 10 mM $Co(NO_3)_2$ and 10 mM $NaNO_3$ were dissolved in 20.0 mL of deionized water to form homogeneous solution. Then 10 mL $NH_3 \cdot H_2O$ was added dropwise to the mixed solution with constant stirring in air for about 30 mins. After the addition of 4 mL of H_2O_2, subsequently the mixture was sealed in a 200 ml teflon-lined stainless steel autoclave and transferred into a homogeneous reactor set at 120 ℃ for 12 h. By the time the reactor cooled to room temperature, the samples were rinsed three times with deionized water and ethanol, respectively, and dried in a conventional oven. Then the black powders of hollow Co_3O_4 microspheres were obtained.

2.3   Materials characterization

The morphologies and structures of product were analyzed by field emission scanning electron microscope (FE-SEM) and Transmission electron microscopic (TEM). FESEM characterization was performed on a JSM-7600F. TEM investigation was carried out using a high-resolution transmission electron microscope (HR-TEM, JEOL, JEM-2100F) operated at 200 kV. All samples were dispersed in absolute ethanol solution and then dropped on copper gird. Selected area electron diffraction (SAED) was also performed via the previous TEM. The phase purity of the as-prepared sample was characterized by X-ray diffraction (D/max 2550VL/PC) with Cu Kα radiation from 10° to 80° at a scanning rate of 4°/min. The X-ray tube voltage and current were set at 35 kV and 200 mA, respectively. The Raman spectrum of the samples was collected on SenterraR200-L Raman system with 532 nm diode laser excitation at room temperature.

2.4 Electrochemical measurements

The electrochemical studies were performed in a conventional three-electrode system with a KOH electrolyte solution (2 mol/L). The newly produced hollow Co_3O_4 microspheres loaded on nickel foams, a platinum electrode, and a saturated calomel electrode (SCE) were used as the working electrode, counter electrode and reference electrode, respectively. The working electrode was composed of active Co_3O_4 materials (75 wt%), carbon black (15 wt%) and binder (PTFE, 10 wt%). The mixture was first coated onto the surface of a piece of nickel foam sheet (1 cm $\times$ 1 cm), and dried at 65℃ overnight. The sheets with active materials were finally pressed under 14 Mpa to obtain the working electrode. The loading weight of hollow Co_3O_4 microspheres on nickel foam sheet was 0.67 mg/cm^2. The cyclic voltammogram (CV), galvanostatic charge/discharge cycle tests and electrochemical impedance spectroscopy(EIS) were performed on a CHI 660E electrochemical workstation. The EIS measurements were performed from the frequency window of 0.01 to 100 KHz at an open-circuit potential with an ac perturbation of 5 mV.

3. Results and discussion

The morphologies of the as-obtained samples were characterized by field emission scanning electron microscope (FE-SEM) and transmission electron microscope (TEM). The SEM image shows the samples possess homogeneous diameters of ca. 500 nm and most of the samples are of intact spherical morphology (see in Fig. 1a). From the amplified SEM image of broken hollow microspheres in Fig. 1b, we could

evaluate that the shell thickness was about 50 nm. It can be learned from Fig.1c that

the hollow Co_3O_4 microspheres exhibit distinct hollow feature and with a thin-wall

shell. In addition, the high magnification TEM image (as shown in Fig.1d) distinctly

reveals the thin shell trait with the shell thickness about 50 nm. The structures of

hollow Co_3O_4 microspheres were further examined by high-resolution transmission

electron microscopy (HR-TEM) and selected area electron diffraction (SAED). On

one hand, as displayed in Fig. 1e, the d-spacings of the hollow microspheres are

approximately 0.28 and 0.24 nm, correspond to the (220) and (311) planes of cubic

Co_3O_4. The clear lattice fringes indicate that the microspheres are composed of a lot

of nanocrystalline with high crystallinity. The distinctive diffraction rings in Fig. 1f

further confirm their polycrystalline feature, which from the center could determined
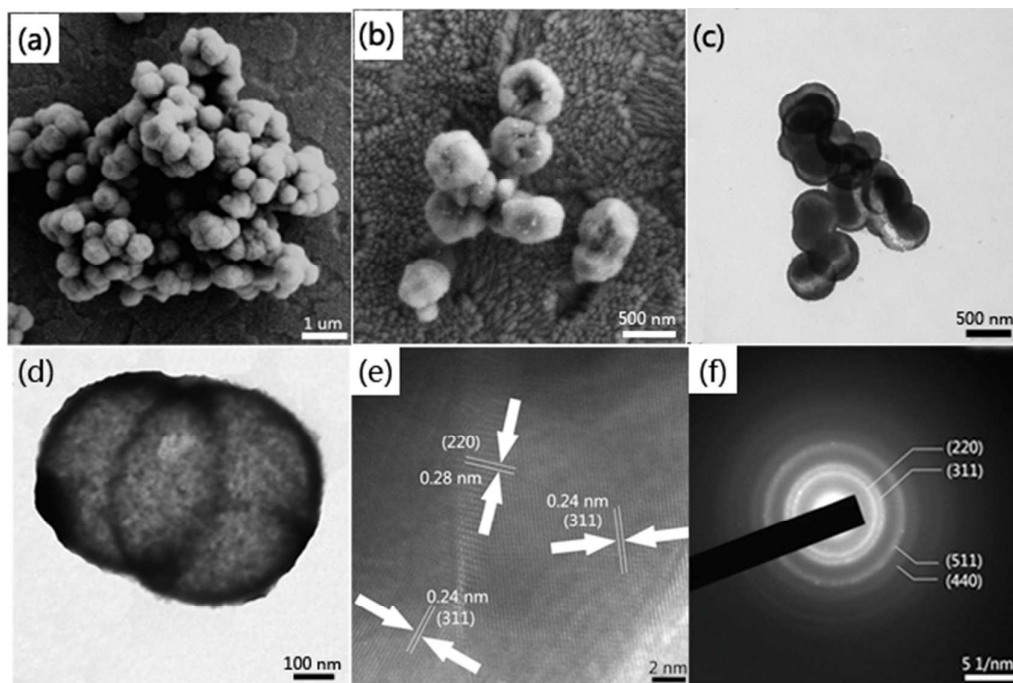
to be (220), (311), (511) and (440) crystal planes.

Fig. 1 (a) Low magnification SEM image of hollow Co_3O_4 microspheres, (b) High

magnification SEM image of broken hollow microspheres, (c) Low magnification

TEM image of hollow Co_3O_4 microspheres, (d) High magnification TEM image of

hollow Co_3O_4 microspheres, (e) HR-TEM image of hollow Co_3O_4 microspheres, (f)

SAED pattern of hollow Co_3O_4 microspheres.

On the other hand, the Raman analysis was also employed to characterize the optical

properties of the hollow Co_3O_4 microspheres. As depicted in Fig. 2a, five apparent

Raman peaks were located at 185, 480, 512, 593, 653 cm^{-1}, respectively. All of these

peaks correspond to three F_{2g} , one E_g, and one A_{1g} Raman-active modes of the Co_3O_4

microcrystals as marked in Fig. 2a. The values are in close proximity to standard

microcrystalline Co_3O_4 powders.[29] This result indicates that the as-prepared samples

are Co_3O_4 crystallizes in the form of the normal spinel structure with $Co^{2+}$and Co^{3+}

being located at the tetrahedral and octahedral sites, respectively. Furthermore,

samples synthesized at different hydrothermal temperatures were characterized by

PXRD analysis. As illustrated in Fig. 2b, all the diffraction peaks could be indexed as

the standard PDF card (JCPDS card No.43-1003) and agree with the characteristics of

cubic spinel Co_3O_4 (Fd3m, a 0 = 8.804Å). There were no diffraction peaks from any

other impurities, which implied the high purity of the Co_3O_4 microspheres. And the

samples obtained at 100 ℃ exhibited poor crystallization properties. However,

accompanied by the rise of hydrothermal temperature, the crystal plane intensity of

(111) which was closely related to Co (II) of spinel Co_3O_4 slightly dropped. On the

contrary, the intensities of (311), (400), (511) and (440) crystal plane related to Co

(III) increased visibly. This phenomenon reflected the fact that higher hydrothermal temperature would accelerate oxidation rate of Co (II). That also explains well why the researchers used to manufacture Co_3O_4 materials with two steps which were composed of synthesis of $Co(OH)_2$ precursor and high temperature calcination oxidation process (> 260 ℃).
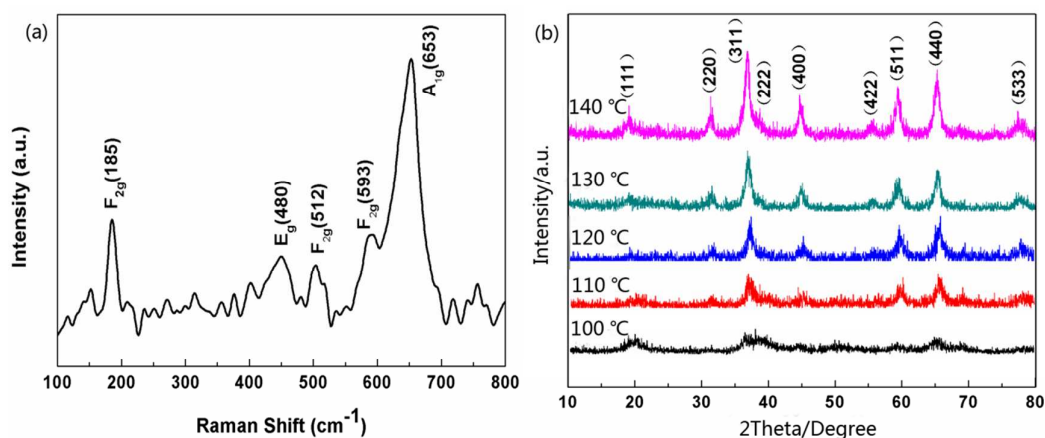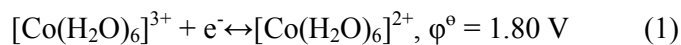

Fig. 2 (a) Raman spectra of hollow Co_3O_4 microspheres, (b) XRD patterns of products which were synthesized at different hydrothermal temperatures.

In this study, to obtain Co_3O_4 in one-step, we introduced cobalt complexes ammonia into the system. Here we shows the corresponding Nernst equations of Co (II) to Co (III) under two totally different reaction conditions:

$$[Co(H_2O)_6]^{3+} + e^- \leftrightarrow [Co(H_2O)_6]^{2+}, \varphi^\ominus = 1.80 \text{ V} \qquad (1)$$

$$[Co(NH_3)_6]^{3+} + e^- \leftrightarrow [Co(NH_3)_6]^{2+}, \varphi^\ominus = 0.18 \text{ V} \qquad (2)$$

Equation (1) represents the general conversion of Co (II) to Co (III) in ordinary alkaline solution. However, while the concentration of NH_3 is comparatively high in the solution, the former ligand (H_2O) of Co^{2+} would inevitably be replaced by NH_3 due to the much bigger coordination stable constant of latter one.[30] Obviously, we

successfully lowered the reaction thermodynamics of this transformation process by introducing NH_3. Therefore, Co_3O_4 materials could be synthesized in one-step with a extremely low hydrothermal temperature (120 ℃).
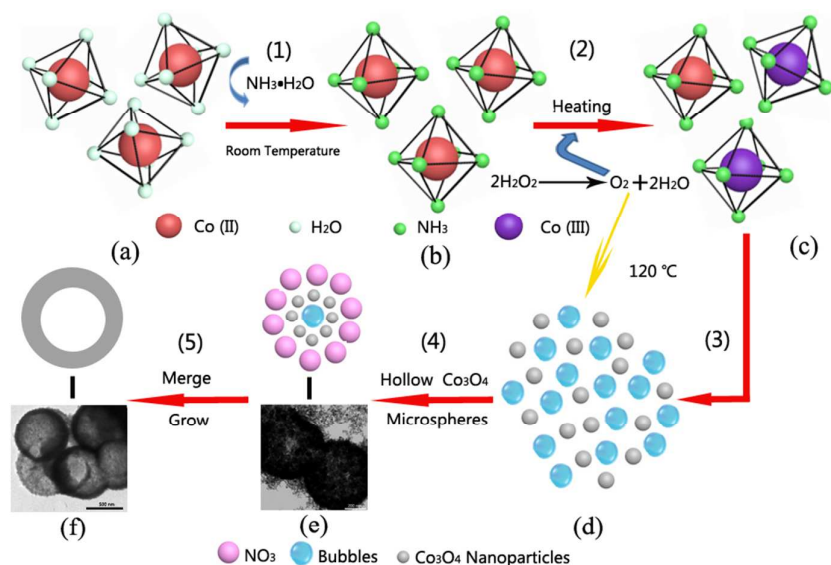

Fig. 3 Formation schematic model of hollow Co_3O_4 microspheres.

Fig. 3 illustrates the synthesis schematic diagram of corresponding hollow Co_3O_4 microspheres. At the step (1), the $[Co(NH_3)_6]^{2+}$ (Fig.3b) would generate at the room temperature. They were rapidly oxidized to $[Co(NH_3)_6]^{3+}$ (Fig. 3c) by O_2 resulted from immediate decomposition of H_2O_2 as illustrated in step (2). Then under the hydrothermal condition, on account of the low coordination stable constant of $[Co(NH_3)_6]^{2+}$ (1.3×10^5),[31] there were simultaneous reactions took place at the same time at step (3). Under this circumstance, massive nanoparticles of Co_3O_4 were produced via the recrystallization process (as displayed in Fig. 3d). In the next place, the O_2 bubbles that were constantly produced due to the decomposition of H_2O_2 serve as center of core-shell structure formation. The vast bubbles consist in the reaction

solution tremendously favor the formation of hollow structure, which kept accordance

with Zhang' work.[38] As shown in the step (4), temporary core-shell structures (Fig.3e)

were formed, and numerous replication products emerged continuously. TEM images

of intermediate products during the preparation process were also shown in Fig. 3e. It

can be seen that the body of hollow Co_3O_4 microspheres were composed of small

Co_3O_4 nanoparticles with size of several nanometers. Take into consideration of the

abundant nitrate co-exsiting in the hydrothermal solution, they would affect the

growth stage by selectively changing the growth kinetics of the different crystals.[32] In

addition, because of the large c-axis distance and charge balance, the nitrate is apt to

insert into the Co-O bond,[33] hence wrapped up Co_3O_4 nanoparticles. As a result, the

disorder attraction of interatomic forces were deliberately interfered, newly-generated

hollow intermediate structure were able to keep evolving *in situ* which isolated to

each other. Under the twin impact of driving force of reducing surface energy and

nitrate, encapsulated Co_3O_4 nanoparticles continued to grow and emerge with

adjacent nanoparticles to forming hollow microspheres (Fig. 3f) as shown in step (5).

Based on the standpoints of formation process mentioned above, H_2O_2 dosage and

nitrate concentration seem to play irreplaceable mutual roles on facilitating the

synthesis of hollow Co_3O_4 microspheres. Hence, we carried out two control

experiments to investigate the effect of H_2O_2 and nitrate exerted on the Co_3O_4 crystal

growth. However, the bubbles stemmed from the decomposition of H_2O_2 would serve

as template of inner cavities of microspheres during hydrothermal condition. Taking

into account the situation that a number of O_2 has already been consumed in the

oxidation conversion of $[Co(NH_3)_6]^{2+}$ to $[Co(NH_3)_6]^{3+}$, the H_2O_2 dosage is directly related to the size and quality of microsphere cavity. In a typical synthesis of hollow Co_3O_4 microspheres, the H_2O_2 dosage is 4 mL. However, the inadequate H_2O_2 dosage would lead to the fabrication of solid microspheres rather than hollow ones. Fig. 4a,b represents the TEM image of microsphere with the H_2O_2 dosage of 2 mL. The formation of solid Co_3O_4 microspheres (as shown in Fig.4b) is an evident that insufficient bubbles were unqualified for acting as the cavity template. While the H_2O_2 dosage was increased to 3 mL, hollow Co_3O_4 microspheres started to emerge and coexist with solid Co_3O_4 microspheres in final product as shown in Fig. 4c. Combined with the TEM image of Fig. 4d, it is observed that inner cavities were unevenly distributed due to bubbles deficiency. On the other hand, excess H_2O_2 would also brought negative effect into the synthesis process. As seen in Fig. 4e and 4f that although bubbles could act as the template of hollow structure, there was also a side-effect which can not be ignored. Disturbance of bubbles aggravated due to the increase of H_2O_2 (5 mL), which caused severe damages to the formation and growth of shell structures (as shown in Fig.4e). In this case, a large number of shell fragments coexisted with the integrated hollow microspheres in the final products. As the augment tendency of H_2O_2 dosage (6 mL) continued, a tremendous amount of bubbles would totally destroy the hollow structures, and as a result, blocky-shaped particles with voids generated instead of hollow Co_3O_4 microspheres (as displayed in Fig. 4g).
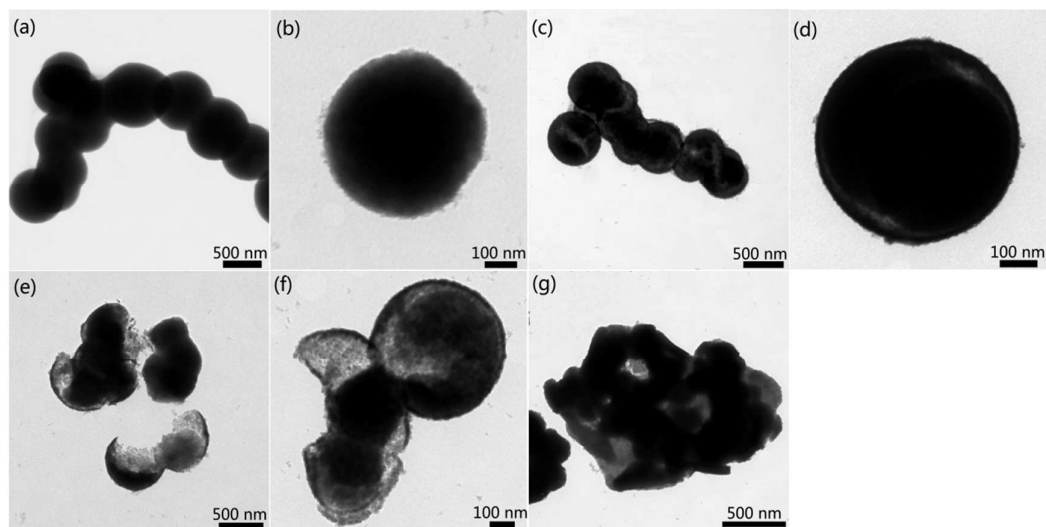
Fig. 4 (a) Low magnification TEM image of microspheres with H_2O_2 dosage of 2 mL; (b) High magnification TEM image of individual solid microsphere with H_2O_2 dosage of 2 mL; (c) Low magnification TEM image of microspheres with H_2O_2 dosage of 3 mL; (d) High magnification TEM image of hollow Co_3O_4 microsphere with small cavity with H_2O_2 dosage of 3 mL; (e) Low magnification TEM image of microspheres with H_2O_2 dosage of 5 mL; (f) High magnification TEM image of cracked hollow Co_3O_4 microsphere with H_2O_2 dosage of 5 mL; (g) TEM image of product with H_2O_2 dosage of 6 mL.

Fig. 5 shows the TEM images of various samples, which were prepared with different nitrate concentrations but keep other parameters constant. It can easily be seen from Fig. 5a that the severe deficiency of nitrate (0.5 M) are unable to cover all the newly-produced Co_3O_4 nanocrystals in this situation. As a result, in spite of inner cavity caused by bubbles, the majority of nanocrystals reunited with each other to grow into blocky-shaped particles with voids (as shown in Fig.5b). Accompanied by

the increase of nitrate concentration (0.75 M), agglomerate phenomena were alleviated to some extent. As seen in Fig. 5c, incremental nitrate promoted the trend of hollow microspheres formation. With the assistance of nitrate inserting into Co-O bond, a substantial part of particles were of spherical morphology. Fig. 5d shows the TEM image of twin hollow microspheres that sharing the same internal cavity. The nitrate concentration of 1 M adopted in the typical synthesis process as shown in experimental section turned out to be optimum parameter that most benefits the preparation of hollow Co_3O_4 microspheres. As the concentration continued to increase, the amount of nitrate surpassed the appropriate dosage needed for covering Co_3O_4 microspheres with uniform size of 500 nm. As shown in Fig. 5e, some of the hollow Co_3O_4 microspheres possess bigger size than 500 nm and a magnified hollow Co_3O_4 microsphere shows the diameter of ca. 550 nm (as shown in Fig.5f). While the concentration of nitrate was increased to 1.5 M, the size of these as-obtained hollow Co_3O_4 microspheres were no longer homogeneous as shown in Fig. 5g and 5h, which could surely ascribed to the superfluous nitrate. Because under the hydrothermal condition, excess nitrate provided bigger cladding surface area for Co_3O_4 microspheres thus weakened the size restriction in the process of Co_3O_4 nanocrystals growth.
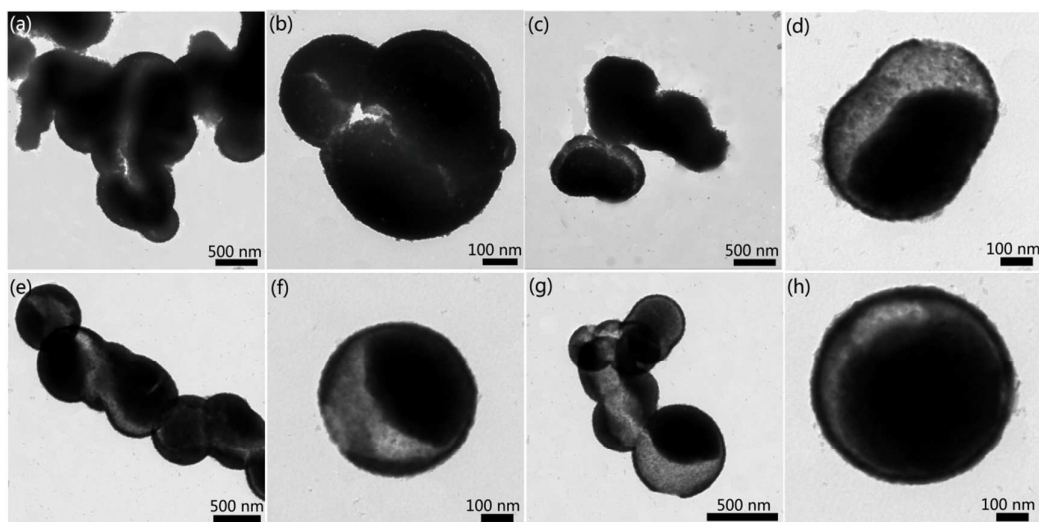
Fig. 5 (a), (c), (e), (g) TEM image and (b), (d), (f), (h) high magnification image of the as-prepared samples with nitrate concentration at 0.5, 0.75, 1.25, 1.5 M, respectively.

The electrochemical performances of the as-obtained hollow Co_3O_4 microspheres were investigated by CV, galvanostatic charge/discharge tests and EIS. The CVs of the hollow Co_3O_4 microspheres were recorded at different scan rates and in a potential range of -0.25 ~ 0.55 V (*vs.* SCE). All the curves show obvious pseudocapacitance features with a similar line type as shown in Fig. 6a. It can be observed in the graph that cathodic scan of CV curves did not match well with the corresponding anodic ones, which declares the polarizations exist in Faradaic redox reactions.[34]

The pseudo-capacitances of the hollow Co_3O_4 microspheres were elucidated by galvanostatic charge/discharge tests in the potential range of 0 ~ 0.47 V. The specific capacitance of the supercapacitors could be evaluated from the charge/discharge tests together with the following equation:[35]

$$C_m = I\Delta t / m\Delta V \qquad\qquad (3)$$

where C_m is the specific capacitance of the capacitor (F/g) , I is the current of

charge/discharge, and Δt is the discharge time period for the potential change ΔV, in

volts, m is the mass load of the active material in electrode. Fig. 6b and Fig.6c shows

the charge/discharge curves and specific capacitance values of pseudocapacitors made

with as-prepared hollow Co_3O_4 microspheres measured at different current densities.

The specific capacitance of hollow Co_3O_4 microspheres was calculated to be 1227,

1169, 1116, 1035 F/g for various current density set at 1, 2, 4, 8 A/g, respectively. The

dramatic performance advantage of hollow Co_3O_4 microspheres was attributed to the

unique hollow nanostructure with thin shell which greatly increased the specific

surface area of electrode materials. In this way, the active sites were more accessible

to electrolytes and charge diffusion distances were largely shortened. However, in

Wang's latest work,[36] they declared the synthesis of 3D-nanonet hollow structured

Co_3O_4 nanomaterials at comparatively low temperature, even in a high concentration

KOH solution (6 M), the sample exhibited a highest specific capacitance of 820 F/g at

different scan rates. In a period of time ago, Meher also obtained ultralayered Co_3O_4

nanostructures with the specific capacitance of 548 F/g.[37] The great improvement of

maximum specific capacitance of hollow Co_3O_4 microspheres over 3D-nanonet

hollow structured Co_3O_4 nanomaterials and ultralayered Co_3O_4 nanostructures could

ascribed to two main aspects. Firstly, the thin shell with nanoscale thickness not only

benefited the ion transport but also provided far more electrochemical active sites than

traditional nanostructures. Therefore, the efficiency of electrochemical reactions

increases dramatically. Secondly, the shell were relatively fragile due to their ultrathin thickness, they would inevitably be broken in preparation and subsequent post-treatment process, which could be supported by TEM images in both Figure 1a, 1b. In this way, the potential accessible active sites of hollow Co_3O_4 microspheres became even more.
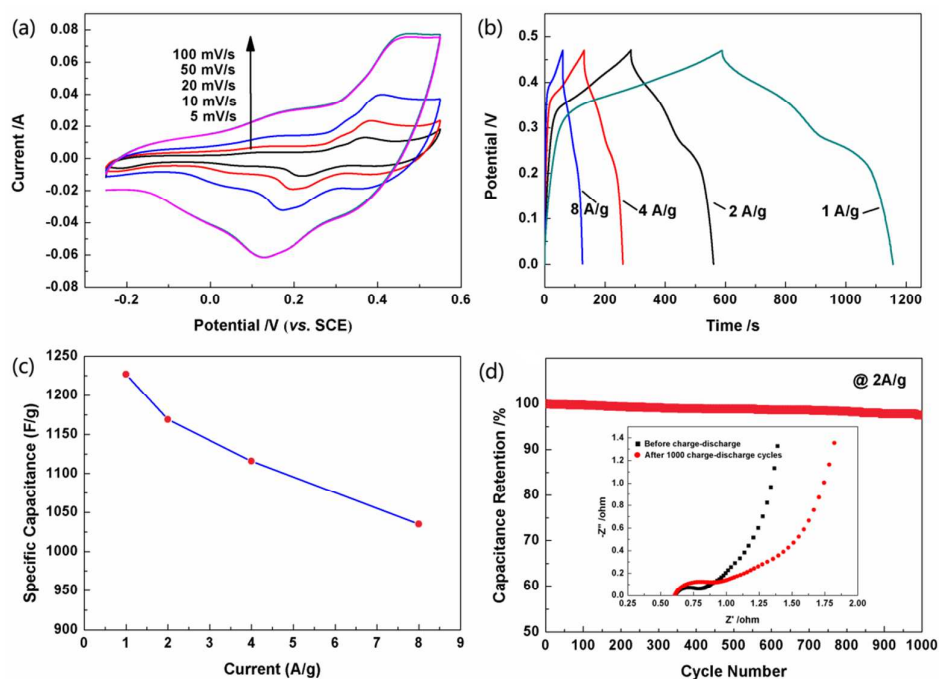

Fig. 6 (a) The CV curves of the hollow Co_3O_4 microspheres recorded at different scan rates. (b) The first time charge/discharge curves of the hollow Co_3O_4 microspheres measured at different current densities. (c) Specific capacitance values of hollow Co_3O_4 microspheres at different current densities. (d) Specific capacitance versus cycle number of hollow Co_3O_4 microspheres at a galvanostatic charge and discharge current density of 2 A/g. The inset is EIS spectras of hollow Co_3O_4 microspheres before and after 1000 cycles.

Cycling stability is another key index for the supercapacitors possess application

potentials. As seen in Fig. 5d, after cycling for 1000 times, the capacitance of electrode made of hollow Co_3O_4 microspheres only slightly decreased to approximately 97.5% of its maximum value, which indicated its excellent reversibility. This result also consisted with the EIS curve in Fig.6d inset. Obviously the internal resistance of the solution almost remained the same after the cycling test, and the charge transfer resistance undergone a slight increase. The internal cavity of hollow Co_3O_4 microspheres could provide buffer for the thermal expansion during electrochemical process. And thin shell of hollow Co_3O_4 microspheres also are in favor of keeping solution evenly by facilitating ion transport. Therefore, even after a long cycle of 1000 times, the electrode structure basically kept intact.

4. Conclusions

In this report, hollow Co_3O_4 microspheres with thin shell of 50 nm were synthesized with one-step hydrothermal method in low temperature (120 ℃). By means of taking advantages of mutual influences of nitrate and H_2O_2, hollow Co_3O_4 microspheres with thin shell were obtained for the first time with the absence of morphology template, organic reagent and additional calcination. Subsequent electrochemical evaluation showed that hollow Co_3O_4 microspheres possess a maximum specific capacitance of 1227 F/g and 97.5 % of the initial value even after a long cycling test of 1000 times. This tremendous superiority could be ascribed to its hollow nanostructure and thin shell, which not only greatly increased the active sites of electrode materials and shortened ion transfer distance but also offered buffer for the thermal expansion

during electrochemical process. This study projected a light beam on the novel thought of synthesis control of nanostructure relying on managing micro-reaction conditions.

AUTHOR INFORMATION

Corresponding Author

* E-mail: (Y.D.D.) yida.deng@tju.edu.cn

* E-mail: (W.B.H.)wbhu@263.net

Acknowledgements

Notes and references

1. G. P. Wang, L. Zhang and J. J. Zhang, *Chemical Society Reviews*, 2012, 41, 797-828.
2. J. B. Goodenough and K. S. Park, *Journal of the American Chemical Society*, 2013, 135, 1167-1176.
3. W. Q. Zeng, F. P. Zheng, R. Z. Li, Y. Zhan, Y. Y. Li and J. P. Liu, *Nanoscale*, 2012, 4, 2760-2765.
4. Y. Zhang, B. Cui, O. Derr, Z. B. Yao, Z. T. Qin, X. Y. Deng, J. B. Li and H. Lin, *Nanoscale*, 2014, 6, 3376-3383.
5. X. Li, W. Sun, L. Wang, Y. Qi, T. Guo, X. Zhao and X. Yan, *RSC Advances*, 2015, 5, 7976-7985.
6. K. Shi and I. Zhitomirsky, *RSC Advances*, 2015, 5, 320-327.
7. M. Kuang, Y. X. Zhang, T. T. Li, K. F. Li, S. M. Zhang, G. Li and W. Zhange, *J. Power Sources*, 2015, 283, 270-278.
8. G. Nagaraju, Y. H. Ko and J. S. Yu, *J. Power Sources*, 2015, 283, 251-259.
9. P. Yan, R. Zhang, J. Jia, C. Wu, A. Zhou, J. Xu and X. Zhang, *J. Power Sources*, 2015, 284, 38-43.

10. H. Jiang, T. Zhao, C. Y. Yan, J. Ma and C. Z. Li, *Nanoscale*, 2010, 2, 2195-2198.

11. H. L. Wang, H. S. Casalongue, Y. Y. Liang and H. J. Dai, *Journal of the American Chemical Society*, 2010, 132, 7472-7477.

12. T. M. Dinh, A. Achour, S. Vizireanu, G. Dinescu, L. Nistor, K. Armstrong, D. Guay and D. Pech, *Nano Energy*, 2014, 10, 288-294.

13. C. Zhang, Y. Xie, M. Zhao, A. E. Pentecost, Z. Ling, J. Wang, D. Long, L. Ling and W. Qiao, *ACS Applied Materials and Interfaces*, 2014, 6, 9751-9759.

14. X. Wang, S. Yao, X. Wu, Z. Shi, H. Sun and R. Que, *RSC Advances*, 2015, 5, 17938-17944.

15. F. Luan, G. M. Wang, Y. C. Ling, X. H. Lu, H. Y. Wang, Y. X. Tong, X. X. Liu and Y. Li, *Nanoscale*, 2013, 5, 7984-7990.

16. M. B. Zakaria, M. Hu, R. R. Salunkhe, M. Pramanik, K. Takai, V. Malgras, S. Choi, S. X. Dou, J. H. Kim, M. Imura, S. Ishihara and Y. Yamauchi, *Chemistry - A European Journal*, 2015, 21, 3605-3612.

17. M. K. Liu, W. W. Tjiu, J. S. Pan, C. Zhang, W. Gao and T. X. Liu, *Nanoscale*, 2014, 6, 4233-4242.

18. M. Pang, G. Long, S. Jiang, Y. Ji, W. Han, B. Wang, X. Liu and Y. Xi, *Electrochim. Acta*, 2015, 161, 297-304.

19. B. R. Duan and Q. Cao, *Electrochim. Acta*, 2012, 64, 154-161.

20. S. L. Xiong, J. S. Chen, X. W. Lou and H. C. Zeng, *Advanced Functional Materials*, 2012, 22, 861-871.

21. J. Zhang, W. Gao, M. Dou, F. Wang, J. Liu, Z. Li and J. Ji, *Analyst*, 2015, 140, 1686-1692.

22. M. Chen, X. Xia, J. Yin and Q. Chen, *Electrochim. Acta*, 2015, 160, 15-21.

23. Y. H. Xiao, A. Q. Zhang, S. J. Liu, J. H. Zhao, S. M. Fang, D. Z. Jia and F. Li, *J. Power Sources*, 2012, 219, 140-146.

24. R. Edla, N. Patel, M. Orlandi, N. Bazzanella, V. Bello, C. Maurizio, G. Mattei, P. Mazzoldi and A. Miotello, *Applied Catalysis B: Environmental*, 2015, 166-167, 475-484.

25. Y. H. Xiao, S. J. Liu, F. Li, A. Q. Zhang, J. H. Zhao, S. M. Fang and D. Z. Jia, *Advanced Functional Materials*, 2012, 22, 4052-4059.

26. M. X. Liao, Y. F. Liu, Z. H. Hu and Q. Yu, *Journal of Alloys and Compounds*, 2013, 562, 106-110.

27. J. M. Ma and A. Manthiram, *Rsc Advances*, 2012, 2, 3187-3189.

28. H. T. Sun, X. Sun, T. Hu, M. P. Yu, F. Y. Lu and J. Lian, *J. Phys. Chem. C*, 2014, 118, 2263-2272.

29. V. G. I. Hadjiev, M.N.; Vergilov, I.V., *Journal of Physics C (Solid State Physics)* 1998, 21.

30. X. H. Xia, J. P. Tu, Y. J. Mai, X. L. Wang, C. D. Gu and X. B. Zhao, *Journal of Materials Chemistry*, 2011, 21, 9319-9325.

31. W. Y. Sun, *Chemical Industry Press, Beijing*, 2010.

32. L. W. Qian, J. T. Zai, Z. Chen, J. Zhu, Y. P. Yuan and X. F. Qian, *Crystengcomm*, 2010, 12, 199-206.

33. H. Zhang, J. B. Wu, C. X. Zhai, X. Y. Ma, N. Du, J. P. Tu and D. R. Yang, *Nanotechnology*, 2008, 19.

34. S. K. Meher, P. Justin and G. R. Rao, *Nanoscale*, 2011, 3, 683-692.

35. M. S. Wu, Y. A. Huang and C. H. Yang, *Journal of the Electrochemical Society*, 2008, 155, A798-A805.

36. Y. Y. Wang, Y. Lei, J. Li, L. Gu, H. Y. Yuan and D. Xiao, *ACS Appl. Mater. Interfaces*, 2014, 6,

6739-6747.

37.   S. K. Meher and G. R. Rao, *J. Phys. Chem. C*, 2011, 115, 15646-15654.